Applied Physics Letters

Structural and optical properties of nonpolar *m*- and *a*-plane GaN/AlGaN heterostructures for narrow-linewidth mid-infrared intersubband transitions

Cite as: Appl. Phys. Lett. **116**, 201103 (2020); https://doi.org/10.1063/1.5143785
Submitted: 06 January 2020 . Accepted: 24 April 2020 . Published Online: 18 May 2020

Morteza Monavarian, Jiaming Xu, Micha N. Fireman, Nishant Nookala, Feng Wu, Bastien Bonef, Kai S. Qwah, Erin C. Young, Mikhail A. Belkin, and James S. Speck

Applied Physics Letters ARTICLE scitation.org/journal/apl

Structural and optical properties of nonpolar *m*- and *a*-plane GaN/AlGaN heterostructures for narrow-linewidth mid-infrared intersubband transitions

Cite as: Appl. Phys. Lett. **116**, 201103 (2020); doi: 10.1063/1.5143785
Submitted: 6 January 2020 · Accepted: 24 April 2020 ·
Published Online: 18 May 2020

Morteza Monavarian,[1,a] Jiaming Xu,[2] Micha N. Fireman,[1] Nishant Nookala,[2] Feng Wu,[1] Bastien Bonef,[1] Kai S. Qwah,[1] Erin C. Young,[1] Mikhail A. Belkin,[2,3] and James S. Speck[1]

AFFILIATIONS

[1]Materials Department, University of California, Santa Barbara, California 93106, USA
[2]Electrical and Computer Engineering Department, University of Texas, Austin, Texas 78758, USA
[3]Walter Schottky Institut, Technische Universität München, Am Coulombwall 4, 85748 Garching, Germany

[a)]Author to whom correspondence should be addressed: mmonavarian@ucsb.edu

ABSTRACT

Mid-infrared intersubband transitions are investigated in nonpolar *m*-plane and *a*-plane GaN/AlGaN multi-quantum well heterostructures. Nominally identical heterostructures were grown by ammonia molecular-beam epitaxy on free-standing *m*-plane and *a*-plane GaN substrates. A total of 12 well- and barrier-doped samples with intersubband transition energies in the range of 220–320 meV (wavelength range 3.8–5.6 μm) were grown. The intersubband absorption lines of the *m*-plane samples were 10–40% narrower than those of the *a*-plane samples, and a very narrow intersubband absorption linewidth of 38 meV (full width at half maximum) at a transition energy of approximately 250 meV (5 μm wavelength) was observed in an *m*-plane sample. Narrower intersubband absorption linewidths of *m*-plane samples can be explained by more abrupt heterostructure interfaces revealed by structural characterization, which is attributed to a higher stability of the *m*-plane compared to the *a*-plane. No significant difference in the intersubband absorption linewidth was observed between the barrier- and well-doped samples.

III-nitride heterostructures have shown significant progress in various applications within optoelectronics, photonics, and power electronics.[1,2] More recently, III-nitride heterostructures have attracted a great deal of attention for emerging intersubband (ISB) devices to potentially encompass both infrared (IR) and terahertz (THz) spectra. The large conduction band offsets,[3] ultrafast electron relaxation times,[4,5] and high longitudinal optical (LO) phonon energy (~92 meV)[1] have made III-nitrides particularly unique for the development of short-wavelength IR (SWIR, $\lambda \approx$ 1.4–3 μm) and THz ($\lambda \approx$ 30–300 μm) ISB devices[6,7] for telecommunication, biological applications, pharmaceutical quality control, and security screening.[8] The THz sources are typically made by GaAs-based quantum-cascade lasers (QCLs) for frequencies < 5 THz.[9,10] However, due to the issues with phonon absorption in the GaAs material system, higher frequencies (5–10 THz) have been difficult to reach by this system. Additionally, relatively small LO phonon energy in GaAs leads to strong deterioration of THz QCL performance at elevated temperatures due to LO phonon scattering of thermal electrons in the upper lasing state.[10] Significantly higher LO phonon energy for III-nitrides may provide a pathway toward room temperature QCLs across the entire THz spectral range.[10]

So far, many of the reported III-nitride ISB structures have been on the polar *c*-plane.[11–13] Despite the great promise of nitrides for ISB devices, the conventional *c*-plane orientation of GaN features a large polarization field that reduces the transition oscillator strength.[14] In addition, the internal electric fields, due to electrical polarization discontinuities, may result in tunneling of the excited carriers through the triangular wells and reduce the transition efficiency.[14] Finally, the energy levels for the bound states in the quantum wells (QWs) are very sensitive to the large electric fields in the heterostructures. Growing the heterostructures on nonpolar orientations, in contrast, would potentially overcome the issues with the conventional polar *c*-plane.[15]

Two low-index nonpolar planes exist in the wurtzite nitride crystal structure, the nonpolar {10–10} family of *m*-planes and the nonpolar {11–20} family of *a*-planes.[16] ISB transitions in nonpolar *m*-plane GaN-based heterostructures have been reported by several groups.[17–22] There is one report of a single ISB structure grown on *a*-plane GaN buffer on *r*-plane sapphire substrates with a very broad ISB transition linewidth of over 100 meV.[23] However, no systematic comparison of identical heterostructures grown on *a*-plane and *m*-plane orientations has been reported so far. One potential reason for fewer available reports on *a*-plane ISB structures compared to the *m*-plane may be the lower stability of the *a*-plane compared to the *m*-plane, resulting in less abrupt interfaces and thus broadened ISB transition peaks. Lim *et al.*[24] have presented investigation of GaN/AlGaN structures on *a*-, *m*-, and *c*-plane GaN substrates designed for ISB transitions in the range of 1.5–2.9 μm. However, the *a*-plane sample morphology was poor, and only one of the *a*-plane samples with very thin GaN QWs (~1.3 nm) in that report displayed a clear ISB absorption peak.[24] For that particular sample, the transition energy and linewidth were very similar to those of an identical structure grown on *m*-plane GaN; however, unlike samples grown on *m*- or *c*-plane substrates, all the other samples grown on *a*-plane GaN did not display clear ISB transitions in that report.[24] Other than these few studies, there are no clear reports that resolve the preferred nonpolar orientation to use for ISB optoelectronics. Hence, a comprehensive study of ISB structures on both *a*-plane and *m*-plane ISB structures is necessary for THz optoelectronics.

In this work, we perform a systematic comparison of ISB transitions in identical nonpolar *m*-plane and *a*-plane GaN/AlGaN heterostructures grown on high-quality free-standing substrates for IR optoelectronics. Identical nonpolar *m*-plane and *a*-plane multi-QW (MQW) structures are compared with various QW widths and doping profiles that result in ISB absorption in the range of 3.8–5.6 μm (220–320 meV or 50–80 THz). The samples were grown by ammonia-molecular beam epitaxy (NH_3-MBE), which have provided more controllable and abrupt interfaces compared to many other available growth techniques.[25] Optical measurements reveal that ISB absorption peaks of the *m*-plane samples are 10–40% narrower than those for *a*-plane samples, due to slightly more abrupt interfaces as indicated by structural characterizations. A record ISB absorption linewidth of ~38 meV at 4.5–5.5 μm was measured on *m*-plane orientation. The results of the ISB absorption match well with structural characterization such as scanning transmission electron microscopy (STEM) and atom-probe tomography (APT).

A Veeco Gen 930 NH_3-MBE system was employed to grow the structures. 20 pairs of GaN/$Al_{0.5}Ga_{0.5}N$ heterostructures were grown on *a*-plane (1° off toward the *c*-direction) and *m*-plane (5° off toward the *a*-direction) stacking-fault-free freestanding substrates with low dislocation densities ($<10^6$ cm^{-1}) from Mitsubishi Chemical Corporation (MCC). More details regarding the growth can be found in the supplementary material. The optimum crystal miscut for each orientation was determined by systematic studies of the surface morphology for growth on substrates with different miscuts, as discussed in the supplementary material.

The schematics of the structures are shown in Fig. 1(a). For this investigation, two separate *n*-type doping profiles were employed to investigate the effects of modulation doping on the ISB optical transition linewidth: well-doped (WD) and barrier-doped (BD). For the WD structures, the QWs were uniformly doped by Si up to ~1.2×10^{19} cm^{-3}, while the quantum barriers (QBs) were unintentionally doped (UID). For the BD structures, the $Al_{0.5}Ga_{0.5}N$ QBs were Si doped by up to ~2×10^{19} cm^{-3}, while the QWs were UID. For the BD samples, to avoid interface roughness induced by high doping, a special doping profile was used: the first 5 Å UID layer was followed by 20 Å doping ([Si]: 2×10^{19} cm^{-3}) and capped with another 5 Å of UID QB, as shown in Fig. 1(a). For each doping profile, three different samples with nominal QW widths of (1) 3.0 nm, (2) 3.3 nm, and (3) 3.7 nm were grown (all QWs are thicker than those reported by Gmachl and Ng[23]). All the thicknesses, doping levels, and compositions were separately calibrated using SIMS and high-resolution x-ray diffraction (HRXRD) on separate calibration samples.

High-angle annular dark-field (HAADF) STEM and APT were used to evaluate the interface quality, compositions, and thicknesses. ISB optical absorption spectra of the samples were then measured using a Fourier-transform IR (FTIR) spectroscopy transmission setup schematically shown in Fig. 1(b). An example of the optical data obtained using this setup is shown in Fig. 1(c). More details regarding the sample preparation and experimental details of STEM, APT, and ISB absorption measurements can be found in the supplementary material.

Figure 1(d) shows an example of the computed band structure of a BD sample with the squares of electron wavefunctions shown for the first two energy levels. The computed transition energies and their comparison to experimental data are given in Table I. For the calculations, we have used the material parameters given in Ref. 26, specifically, electron effective masses of $0.22m_0$ and $0.275m_0$ for the GaN QWs and $Al_{0.5}Ga_{0.5}N$ QBs, respectively (where m_0 is the free electron mass) and the conduction band offset between the QW and QB materials of 0.707 eV. We have neglected non-parabolicity and included many-body effects of exchange and correlation, depolarization, and exciton-like correction following the approach described in Ref. 27. The exchange-correlation correction was computed perturbatively using the expression obtained with the local-density approximation in Ref. 28 with the parameters given in Ref. 29. We note that this approximation appears to yield a better agreement with the experimental results for the moderate doping densities (~4×10^{12} cm^{-2}) used in our structures[30] compared to the alternative Hartree–Fock evaluation of the exchange energy[31,32] applied to GaN/AlGaN heterostructures.[33]

Figure 2 compares HAADF-STEM images of nonpolar *m*-plane and *a*-plane GaN/AlGaN nominal 3 nm QW BD structures. The QW thicknesses range from ~2.90 to 3.31 nm (3.1 nm on average) and from 2.57 to 3.17 nm (2.87 nm on average) for the *m*-plane and the *a*-plane, respectively, indicating slightly thinner QWs in the *a*-plane sample. In addition, the *a*-plane structure shows more indication of interface roughness along the *c*-direction [Fig. 2(b)] compared to the *m*-plane structure with more abrupt interfaces [Fig. 2(a)], potentially due to the higher stability of the *m*-plane compared to the *a*-plane demonstrated earlier.[34–38] The slight diffuseness at the interfaces of the *a*-plane AlGaN/GaN heterostructure is also revealed by APT analysis as shown in Fig. 3. According to the APT data on a selected *a*-plane sample, the top interfaces between the GaN and AlGaN layers are sharp, while the bottom interfaces are less abrupt. Figure 3(b) reports the variation of the Al/(Al+Ga) and Ga/(Al+Ga) ratios along the growth axis in Fig. 3(a). The plateau Al fraction in the AlGaN layers ranges from 52% to 60%, with a deviation of ~3%. A Gaussian

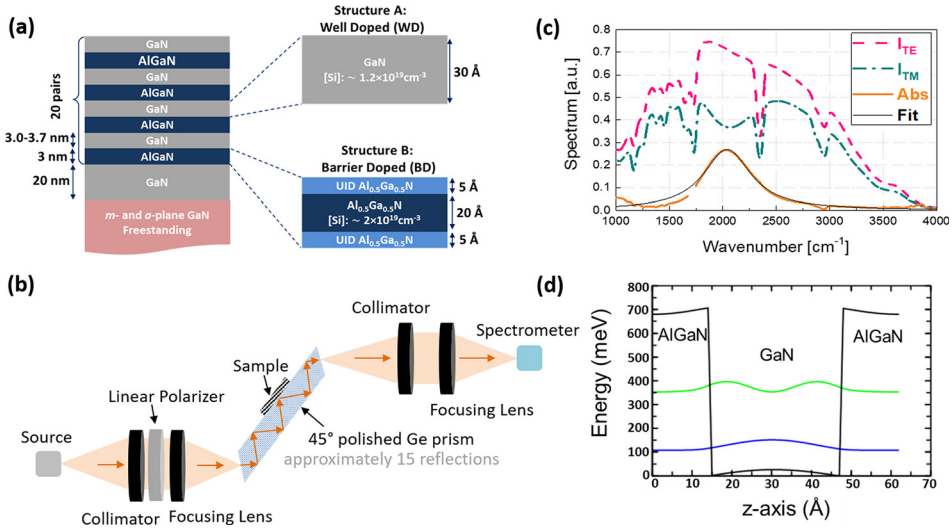

FIG. 1. (a) Cross-sectional schematics of nonpolar *m*-plane and *a*-plane 20 pairs of GaN/$Al_{0.5}Ga_{0.5}N$ ISB heterostructures with a fixed AlGaN QB thickness (3.0 nm) and different GaN QW thicknesses (3.0, 3.3, and 3.7 nm). The doping profile of WD (structure A) and BD (structure B) structures are shown in the right panel of (a). (b) Schematic of the ISB absorption measurement setup. The MQW heterostructure is evanescently illuminated through an IR-transparent germanium prism. The intensity of the transmitted beam is recorded as a function of wavelength. (c) Example of a dataset obtained in the setup in (b). ISB absorption spectra are obtained by measuring the spectral dependence of transmitted intensities for TE-polarized light (I_{TE}, E-field along the surface of the wafer, pink dashed line) and TM-polarized light (I_{TM}, electric field in the plane of incidence, green dashed-dotted line), and then computed as $Log_{10}(I_{TE}/I_{TM})$ (thick orange solid line). Finally, a Lorentz function fitting curve (thin black solid line) is used to determine the spectral position and bandwidth of the ISB absorption band. (d) Calculated conduction band diagram and squares of electron wavefunctions for the ground and the first excited states for a representative BD 3.3 nm-wide GaN/$Al_{0.5}Ga_{0.5}N$ QW structure.

distribution of Al atoms within the AlGaN layer indicates a normal random alloy disorder in the *a*-plane heterostructures. The composition of the *a*-plane AlGaN/GaN structure is confirmed to be ∼55% from APT analysis.

The ISB absorption spectra of the *m*-plane and *a*-plane WD and BD structures are shown in Fig. 4. The results of the measured and calculated ISB transition energies are summarized in Table I. All the structures show a clear decrease in the ISB absorption peak energy with the increasing QW width as expected from quantum-mechanical calculations. All the WD structures show slightly lower ISB energies compared to BD structures for the same QW widths. Slightly larger ISB absorption peak energies were observed in the *a*-plane compared to *m*-plane samples, which may be attributed to the slightly thinner QWs in the *a*-plane, as shown in the STEM results of Fig. 2. The thinner QWs result in larger energy separation between the ground state and the first excited state (larger E_{12}) and thus larger ISB absorption peak energy. Figure 5(a) compares the measured ISB absorption linewidths of all the structures in this study. No significant difference in ISB linewidths was observed between the WD and BD structures. A weak dependence of the ISB linewidth on the QW width was observed for a given substrate orientation. The *m*-plane structures (either WD or BD) show smaller ISB absorption linewidths (in the range of 38–55 meV) compared to the *a*-plane structures (in the range of 58–77 meV), due to the more interface abruptness in the *m*-plane structure as revealed by the STEM evaluation (Fig. 2). The lowest ISB absorption linewidths were measured for the WD *m*-plane structures with the minimum linewidth of ∼38 meV, which is the lowest among any ISB absorption reports in nitride materials.

To compare our results with the other reports in the literature on nitride materials, Fig. 5(b) shows a summary of the dependence of the

TABLE I. Calculated and experimentally measured ISB transition energies (E_{12} in meV) for the BD and WD structures with different QW widths. The calculated values are considered with and without inclusion of many-body effects, and the measured values are given for samples grown on *m*-plane and *a*-plane GaN substrates.

	Barrier-doped (meV)		Theoretical (meV)		Well-doped (meV)		Theoretical (meV)	
	Orientation		Many-body effects		Orientation		Many-body effects	
QW width (nm)	*a*-plane	*m*-plane	No	Yes	*a*-plane	*m*-plane	No	Yes
3.0	329.1	321.9	282.58	311.94	284.5	267.2	289.73	315.26
3.3	294.5	286.5	246.54	278.57	257.4	235.5	253.58	284.81
3.7	253.1	252.7	207.48	243.89	222.3	219.3	214.61	254.98

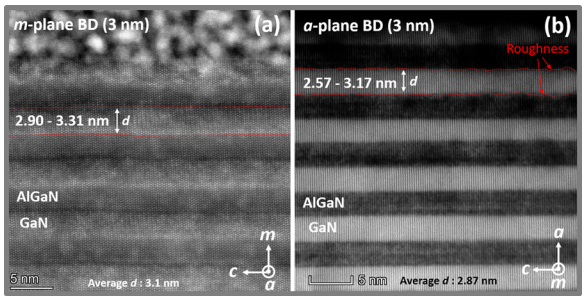

FIG. 2. Cross-sectional high-resolution HAADF-STEM images of (a) nonpolar *m*-plane and (b) *a*-plane 20-pair GaN/$Al_{0.5}Ga_{0.5}N$ (nominal 3.0 nm/3.0 nm) BD heterostructures grown by NH_3-MBE. The images in (a) and (b) are taken across *a*- and *m*-planes, respectively to evaluate the thicknesses and interface abruptness.

ISB optical transition linewidths observed in GaN/AlGaN heterostructures on IR wavelengths ranging from 1.5 μm to ~6 μm. Since the electron density is known to affect the ISB linewidth, we list sheet doping densities for all the structures in the figure. As shown in the figure, the doping densities of our structures are similar to those of most of the structures reported previously. All the average doping levels are within mid to high 10^{18} cm^{-3} ranges, suggesting a fair comparison between the structures. Despite having similar doping densities, the samples presented in this article (open black circles) display the lowest ISB absorption linewidths for nitride-based materials in the mid-IR region. All WD *m*-plane samples demonstrated the record-low ISB absorption linewidths. The record-low ISB linewidths observed in this work are attributed to (i) the flatband condition provided by nonpolar planes and (ii) abrupt interfaces realized by NH_3-MBE growth.

In summary, we have performed growth and characterization of nonpolar *m*-plane and *a*-plane GaN/AlGaN heterostructures designed for the ISB transitions in the mid-IR range. The difference between ISB transition properties of the two nonpolar planes is likely due to more abrupt interfaces, resulting from more stability of the *m*-plane compared to the *a*-plane, as revealed by high-resolution STEM and

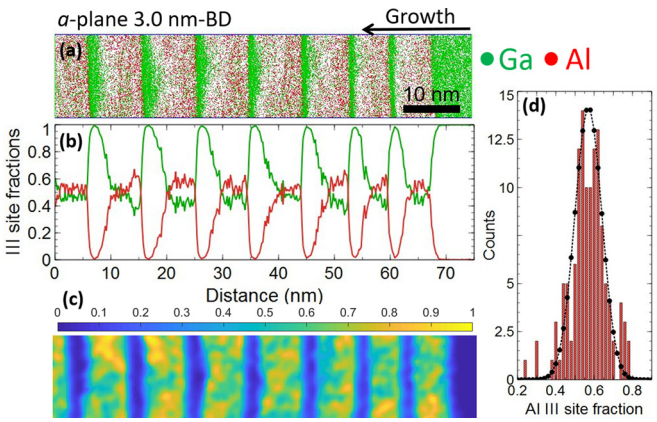

FIG. 3. (a) APT data and analysis of the 20-period nonpolar *a*-plane GaN/AlGaN BD structure with a 3 nm QW width and (b) accompanying line profile of Ga and Al concentrations. (c) Al composition map in the growth direction and (d) distribution of the Al content in the AlGaN QBs. The Al content in the QBs in (d) is binomially distributed, indicative of a random alloy without clustering.

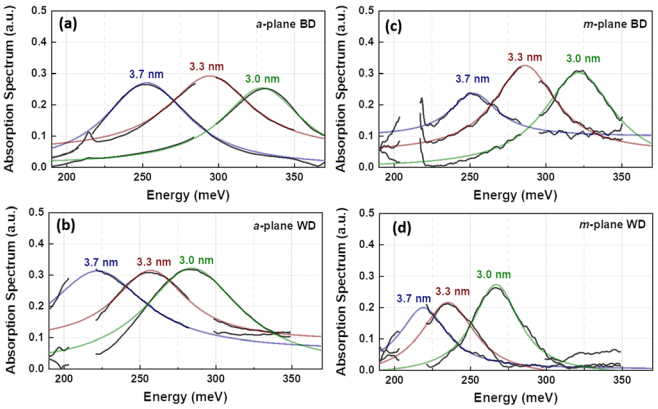

FIG. 4. ISB absorption spectra of (a) *a*-plane BD, (b) *a*-plane WD, (c) *m*-plane BD, and (d) *m*-plane WD GaN/$Al_{0.5}Ga_{0.5}N$ MQW structures. The spectral data in the range of 280–290 meV were omitted due to insufficient light intensity because of a strong CO_2 absorption in air.

APT analysis. A direct comparison of the ISB absorption properties of all the samples reveals that the ISB absorption linewidths for *m*-plane samples are 10%–40% lower compared to those in the *a*-plane samples. A record-low ISB transition linewidth of approximately 38 meV

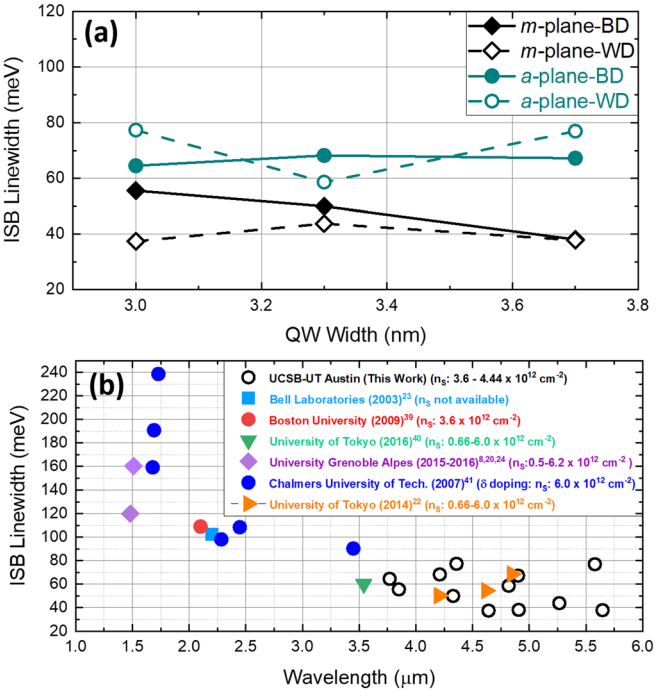

FIG. 5. (a) ISB absorption linewidth as a function of QW width for all the structures used in this study. (b) ISB absorption linewidths vs wavelength for all the data presented in this work (black open circles) compared to other reports of IR ISB transitions in the nitride system in the literature. Our results show the lowest ISB transition linewidths ever reported for GaN-based materials. The data are taken from Refs. 8, 20, 22–24, and 39–41. Sheet doping densities (n_S) for the structures reported by others are included where available for comparison.

was measured for the *m*-plane structures with 3.7 nm QWs. Our results show promise of non-polar GaN/AlGaN MQW heterostructures for the development of ISB devices such as nonlinear optical elements, optical modulators, and QCLs.

See the supplementary material for a more detailed description of the experimental calibrations, measurement setups, and theoretical calculation.

AUTHORS' CONTRIBUTIONS

M.M. and J.X. contributed equally to this work.

This work was supported by the National Science Foundation (NSF) through Grant Nos. ECCS 1809691 and ECCS 1810318. Any opinions, findings, and conclusions or recommendations expressed in this material are those of the author(s) and do not necessarily reflect the views of NSF. The authors acknowledge the support from the Solid-State Lighting and Energy Electronics Center (SSLEEC) at the University of California, Santa Barbara (UCSB). Samples were measured in the Microelectronics Research Center at the University of Texas at Austin, which is a member of the NSF National Nanotechnology Coordinated Infrastructure.

DATA AVAILABILITY

The data that support the findings of this study are available from the corresponding author upon reasonable request.

REFERENCES

[1]H. Morkoç, *Handbook of Nitride Semiconductors and Devices, Materials Properties, Physics and Growth* (John Wiley & Sons, 2009).
[2]D. Feezell and S. Nakamura, C. R. Phys. **19**, 113 (2018).
[3]N. Suzuki and N. Iizuka, Jpn. J. Appl. Phys., Part II **36**, L1006 (1997).
[4]C. Gmachl, S. V. Frolov, H. M. Ng, S.-N. G. Chu, and A. Y. Cho, Electron. Lett. **37**, 378 (2001).
[5]J. Hamazaki, S. Matsui, H. Kunugita, K. Ema, H. Kanazawa, T. Tachibana, A. Kikuchi, and K. Kishino, Appl. Phys. Lett. **84**, 1102 (2004).
[6]E. Bellotti, K. Driscoll, T. D. Moustakas, and R. Paiella, J. Appl. Phys. **105**, 113103 (2009).
[7]G. Sun, J. B. Khurgin, and D. P. Tsai, Opt. Express **21**, 28054 (2013).
[8]C. B. Lim, M. Beeler, A. Ajay, J. Lähnemann, E. Bellet-Amalric, C. Bougerol, J. Schörmann, M. Eickhoff, and E. Monroy, Jpn. J. Appl. Phys., Part 1 **55**, 05FG05 (2016).
[9]R. Köhler, A. Tredicucci, F. Beltram, H. E. Beere, E. H. Linfield, A. G. Davies, D. A. Ritchie, R. C. Iotti, and F. Rossi, Nature **417**, 156 (2002).
[10]B. S. Williams, Nat. Photonics **1**, 517 (2007).
[11]C. Gmachl, H. M. Ng, and A. Y. Cho, Appl. Phys. Lett. **77**, 334 (2000).
[12]J. M. Li, Y. W. Lü, D. B. Li, X. X. Han, Q. S. Zhu, X. L. Liu, and Z. G. Wang, J. Vac. Sci. Technol., B **22**, 2568 (2004).
[13]K. Kishino, A. Kikuchi, H. Kanazawa, and T. Tachibana, Appl. Phys. Lett. **81**, 1234 (2002).
[14]N. Suzuki and N. Iizuka, Jpn. J. Appl. Phys., Part 2 **38**, L363 (1999).
[15]M. Monavarian, A. Rashidi, and D. Feezell, Phys. Status Solidi A **216**, 1800628 (2019).
[16]B. Gil, *Physics of Wurtzite Nitrides Oxides* (Springer, Cham, 2014), pp. 1–48.
[17]D. Feezell, Y. Sharma, and S. Krishna, J. Appl. Phys. **113**, 133103 (2013).
[18]A. Pesach, E. Gross, C.-Y. Huang, Y.-D. Lin, A. Vardi, S. E. Schacham, S. Nakamura, and G. Bahir, Appl. Phys. Lett. **103**, 022110 (2013).
[19]C. Edmunds, J. Shao, M. Shirazi-HD, M. J. Manfra, and O. Malis, Appl. Phys. Lett. **105**, 021109 (2014).
[20]C. B. Lim, A. Ajay, C. Bougerol, B. Haas, J. Schörmann, M. Beeler, J. Lähnemann, M. Eickhoff, and E. Monroy, Nanotechnology **26**, 435201 (2015).
[21]T. D. Moustakas and R. Paiella, Rep. Prog. Phys. **80**, 106501 (2017).
[22]T. Kotani, M. Arita, and Y. Arakawa, Appl. Phys. Lett. **105**, 261108 (2014).
[23]C. Gmachl and H. M. Ng, Electron. Lett. **39**, 567 (2003).
[24]C. B. Lim, M. Beeler, A. Ajay, J. Lähnemann, E. Bellet-Amalric, C. Bougerol, and E. Monroy, J. Appl. Phys. **118**, 014309 (2015).
[25]H. Asahi and Y. Horikoshi, *Molecular Beam Epitaxy: Materials and Applications for Electronics and Optoelectronics* (John Wiley & Sons, 2019).
[26]A. N. Westmeyer, S. Mahajan, K. K. Bajaj, J. Y. Lin, H. X. Jiang, D. D. Koleske, and R. T. Senger, J. Appl. Phys. **99**, 013705 (2006).
[27]M. Helm, in *Semiconductors and Semimetals*, edited by H. C. Liu and F. Capasso (Elsevier, 1999), pp. 1–99.
[28]L. Hedin and B. I. Lundqvist, J. Phys. C **4**, 2064 (1971).
[29]O. Gunnarsson and B. I. Lundqvist, Phys. Rev. B **13**, 4274 (1976).
[30]T. Kotani, M. Arita, and Y. Arakawa, Appl. Phys. Lett. **107**, 112107 (2015).
[31]K. M. S. V. Bandara, D. D. Coon, B. Byungsung, Y. F. Lin, and M. H. Francombe, Appl. Phys. Lett. **53**, 1931 (1988).
[32]K. M. S. V. Bandara, D. D. Coon, B. Byungsung, Y. F. Lin, and M. H. Francombe, Appl. Phys. Lett. **55**, 206 (1989).
[33]T. Nguyen, M. Shirazi-Hosseini-Dokht, Y. Cao, R. E. Diaz, G. C. Gardner, M. J. Manfra, and O. Malis, Phys. Status Solidi A **215**, 1700828 (2018).
[34]B. Imer, F. Wu, M. D. Craven, J. S. Speck, and S. P. DenBaars, Jpn. J. Appl. Phys., Part 1 **45**, 8644 (2006).
[35]B. N. Bryant, A. Hirai, E. C. Young, S. Nakamura, and J. S. Speck, J. Cryst. Growth **369**, 14 (2013).
[36]Q. Sun, C. D. Yerino, B. Leung, J. Han, and M. E. Coltrin, J. Appl. Phys. **110**, 053517 (2011).
[37]Q. Sun, C. D. Yerino, T. S. Ko, Y. S. Cho, I.-H. Lee, J. Han, and M. E. Coltrin, J. Appl. Phys. **104**, 093523 (2008).
[38]D. Du, D. J. Srolovitz, M. E. Coltrin, and C. C. Mitchell, Phys. Rev. Lett. **95**, 155503 (2005).
[39]K. Driscoll, Y. Liao, A. Bhattacharyya, L. Zhou, D. J. Smith, T. D. Moustakas, and R. Paiella, Appl. Phys. Lett. **94**, 081120 (2009).
[40]T. Kotani, M. Arita, K. Hoshino, and Y. Arakawa, Appl. Phys. Lett. **108**, 052102 (2016).
[41]X. Y. Liu, P. Holmström, P. Jänes, L. Thylén, and T. G. Andersson, Phys. Status Solidi B **244**, 2892 (2007).